Variational tolerancing analysis taking thermomechanical strains into account: application to a high pressure turbine

Laurent Pierre
Arts et Metiers ParisTech, I2M, UMR 5295, F-33400 Talence, France.
CNRS, I2M, UMR 5295, F-33400 Talence, France.
Phone : 33 - 5 4000 8790
Fax : 33 - 5 4000 6964
E-mail : laurent.pierre@ensam.eu

Denis Teissandier
Univ. Bordeaux, I2M, UMR 5295, F-33400 Talence, France.
CNRS, I2M, UMR 5295, F-33400 Talence, France.
Phone : 33 - 5 4000 6220
Fax : 33 - 5 4000 6964
E-mail : denis.teissandier@u-bordeaux1.fr

Jean Pierre Nadeau
Arts et Metiers ParisTech, I2M, UMR 5295, F-33400 Talence, France.
CNRS, I2M, UMR 5295, F-33400 Talence, France
Phone : 33 - 5 5684 5428
Fax : 33 - 5 5684 5436
E-mail : jean-pierre.nadeau@ensam.eu

Abstract: The aim of this study is to propose a variational method of tolerancing analysis using a multiphysical approach. This method is based on operations on polytopes (Minkowski sum and intersection) and can be used to validate geometric specifications, contact specifications and thermomechanical specifications.
The first part describes how thermomechanical strains are integrated into a tolerancing analysis tool, based on operations on polytopes. In the second part correlations are defined between two turbine performance criteria, leakage section and risk of touching, and two geometric conditions respectively.
In the third part, the influence of design choices is described, in particular the influence of the shape of the parts and the behaviour of the joints on the thermomechanical operating regime of the turbine.
Two turbine architectures are considered in relation to the same two performance criteria, and lastly the main turbine architecture results are discussed and future developments described.

Keywords: functional dimensioning and tolerancing; variational analysis; thermomechanics; performance criteria; gaz turbine

1. Introduction

Controlling the behaviour and the energy yield of turboshaft engines for each of the different operating regimes is essential to ensure that the desired power is achieved. One way to improve the performance of these turboshaft engines is to control the geometric variability of the turbine, and more particularly the clearance between the blade tips and the stator.

In the preliminary design phase, several alternative turbine architectures are envisaged. These alternatives are often based on different component shapes and dimensions, with several technical solutions being proposed for joints between components and different materials. In this article we propose a model which will define clearance between blade tips and stator for different turbine architectures, taking the following variabilities into account:

- processes for obtaining parts,
- processes for assembling parts,
- thermomechanical behaviour of the turbine.

The model described in this article is based on a variational approach, manipulating sets of geometric constraints that formalise polytopes [1].

A polytope is the bounded intersection of a finite set of closed half-spaces of $\mathbb{R}^n$ of which the boundaries are hyperplanes of $\mathbb{R}^{n-1}$ [2]. A polytope is used to define all the positions of a surface within a tolerance zone (geometric polytope) and all the relative positions between two surfaces potentially in contact (contact polytope). By applying operations (Minkowski sums [3], [4] and intersections) to geometric and contact polytopes it is then possible to characterise the relative position between the rotor and the stator in a turbine. These operations are deduced from the topological structure of the turbine defined by a contact graph for one connected component [5].

There are models that characterise geometric variations by sets of constraints; these include the domain [6], the T-Map [7] and the polyhedron [8]. In contrast to the polytope, in domains and T-Maps the boundaries of the half-spaces are generally not linear.

Clearance between the rotor and the stator in the turbine is defined in terms of a reference model with a reference behaviour. In the reference behaviour, all the parts are at 20°C and are modelled by infinitely rigid solids [9]. In the reference model any geometric variability due to manufacturing and assembly processes can be shown.

The turbine's operating cycle is discretized into several distinct thermomechanical behaviours which correspond respectively to different thermomechanical specifications [10]. No transitional regime is considered. Clearance between the rotor and the stator in the turbine is characterised by a thermomechanical model based on a reference model and incorporating thermomechanical strains in the parts and the contacts. The thermomechanical model is then used to define geometric variability due to manufacturing and assembly processes and also variability inherent in the thermomechanical behaviour of the turbine.

Two performance criteria are formulated with which to qualify the proposed turbine architectures: risk of touching and leakage section between rotor and stator. This work is part of a general series of studies into decision support systems to assist the designer in choosing a qualified turbine architecture that performs better than any other.

In the first part, the procedure for modelling different geometric variabilities is described. In the second part the qualification criteria for turbine architectural solutions are presented. In the third part, we describe an application of this work to a sub-unit of a turbine of turboshaft engine.

Finally, after drawing the principal conclusions, future developments for this work are presented.

2. Modelling geometric variability

The geometric variability in processes for obtaining parts and in assembly processes are taken into account by 3d dimension chain simulation tools. However, most of these tools model the different parts as infinitely rigid solids, so to make up for this, the thermomechanical strains on the parts must be integrated into 3d dimension chain simulations. This is essential in order to control clearance at the tip of the turbine blade in different operating phases in a turboshaft engine [9].

2.1. Variability due to manufacturing and assembly processes

The geometric models used in 3d dimension chains are generally based on the following hypotheses: no defect in the shape of the real surfaces, no local strain on surfaces in contact and no flexible parts. These hypotheses define the reference behaviour of a system. The limits for geometric defects in a part (defined by specification) are defined by a geometric polytope; the acceptable limits for relative displacement between two surfaces in contact (defined by clearance) are defined by a contact polytope. A functional condition expressed between any two surfaces of a mechanism is characterised by a functional polytope. Respecting a functional condition is simulated by including a calculated polytope in the functional polytope [1], [11] and [12]. The calculated polytope is the result of operations (Minkowski sums and intersections) between geometric polytopes and contact polytopes.
Let us consider figure 1a: surfaces 1,2 and 1,3 of part 1 are in contact with surfaces 2,2 and 2,3 of part 2 respectively.

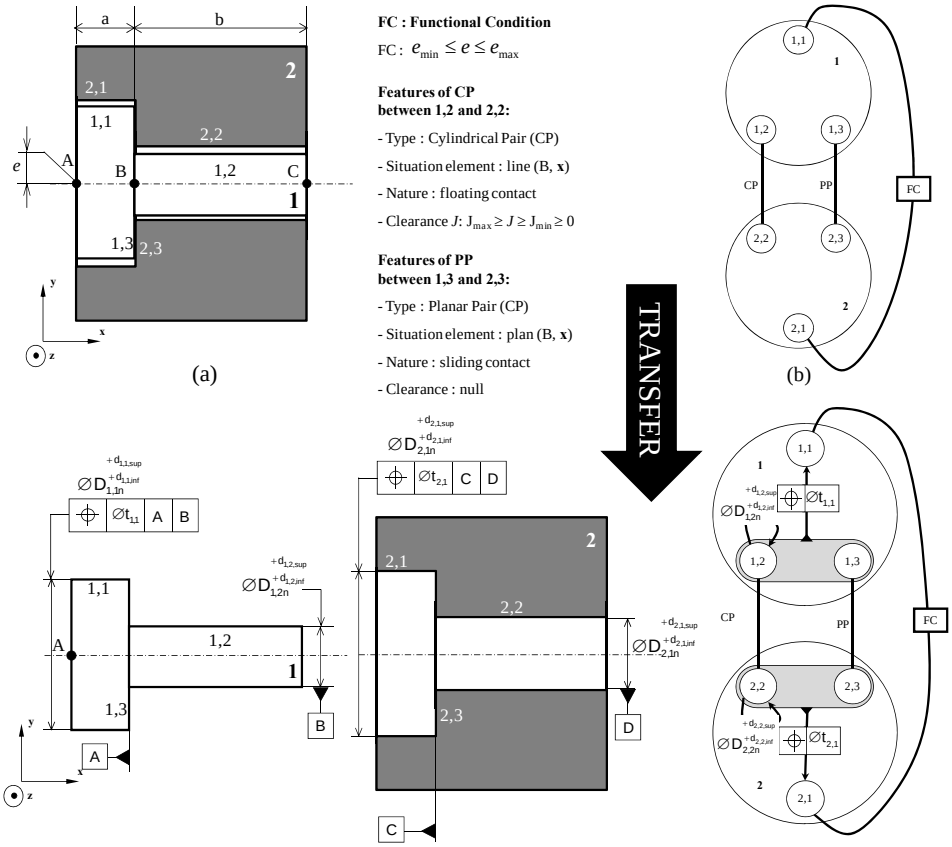

Figure 1: Transfer of FC.

Contact between two surfaces, i.e. a joint, can be defined using a set of parameters. There have been several studies on this subject [13], [14], [15]. Hereafter we will use the definition proposed in [16], which is a direct application of that described in [15].
A joint is defined according to the following parameters:

- type: planar pair, cylindrical pair, ball and cylinder pair, etc.
- situation element(s): plane, straight line, point
- nature: fixed, sliding or floating
- clearance: minimal clearance and maximal clearance: $J_{\min}, J_{\max}$.

The type of joint conforms to those defined in [17] and is determined according to the types of the two surfaces in contact and their relative position.
The situation elements position the joint in space, and thus define the directions of degrees of mobility [5], [18]. A cylindrical pair joint will be defined by a straight line; a planar pair joint by a plane, etc.The nature of the contact determines the behaviour of the joint in the following three configurations: floating, sliding or fixed [15].
In the case of a cylindrical pair joint, ball and cylinder joint or spherical pair joint, clearance is defined as the difference between the diameter of the hole and the diameter of the shaft. Clearance may be positive, null or negative. In the case of a ball and plane pair, cylinder and plane pair or planar pair joint, clearance is the distance between the two surfaces potentially in contact. In this case clearance may be positive or null.
The contacts between surfaces 1,2 and 2,2 and between surfaces 1,3 and 2,3 are defined in figure 1a.
Let us suppose that functional condition FC, limiting the relative position of surfaces 1,1 and 2,1, must be respected. There is coaxiality such that the displacement e of point A on the axis of surface 1,1 in relation to the axis of surface 2,1 respects FC for all directions orthogonal to axis **x**.

$$\mathrm{FC} : \mathrm{e}_{\min} \le e \le \mathrm{e}_{\max} \tag{1}$$

The graph in figure 1b shows the topological structure of the system illustrated in figure 1a. This is sometimes called the joint graph or contact graph [5]. The two parts, 1 and 2, are represented by the two large circles while the surfaces of parts 1 and 2 are represented by the small circles inside the large circles 1 and 2 respectively. The designation i, j inside a small circle means surface j of part i. The two contacts are defined by the two edges linking vertices 1,2 : 2,2 and 1,3 : 2,3 respectively. The functional condition FC is defined by an edge between surfaces 1,1 and 2,1 labelled FC.
In figure 1c, the location specifications for surfaces 1,1 and 2,1 in relation to reference systems A B and C D respectively, are specifications that are influent on the FC. Similarly, the diameter specifications for surfaces 1,2 and 2,2 are also influent on the FC. These specifications are compliant with ISO standards [19], [20] and [21]. Generally, location and diameter specifications are the result of transferring the FC to parts 1 and 2. These specifications are also shown in the graph in figure 1d. In the representation of the two location specifications the point of the arrow indicates the toleranced element while the triangle indicates the reference system. The diameter specifications are intrinsic to surfaces 1,2 and 2,2 and are represented by an arc attached to the same vertex.
In this example, respect for the FC can therefore be defined by the following equation where the calculated polytope, written as $\mathfrak{D}_{1,1/2,1}$, must be included in the functional polytope, written $\mathfrak{D}^{\mathrm{f}}_{1,1/2,1}$:

$$\mathfrak{D}_{1,1/2,1} \subseteq \mathfrak{D}^{\mathrm{f}}_{1,1/2,1} \tag{2}$$

The calculated polytope is defined by equation (3) where:
- $\mathfrak{D}^{g}_{1,1/1,3\text{-}1,2}$ and $\mathfrak{D}^{g}_{2,3-2,2/2,1}$ represent the locations of parts 1 and 2 respectively,

$\mathfrak{D}^{c}_{1,2/2,2}$ and $\mathfrak{D}^{c}_{1,3/2,3}$ represent the cylindrical pair and planar pair joints respectively.

$$\mathfrak{D}_{1,1/2,1} = \mathfrak{D}^{g}_{1,1/1,3\text{-}1,2} + \left(\mathfrak{D}^{c}_{1,2/2,2} \cap \mathfrak{D}^{c}_{1,3/2,3}\right) + \mathfrak{D}^{g}_{2,3-2,2/2,1} \quad (3)$$

The limits for the positions of the surface 1,1 axis in the tolerance zone TZ enable us to define all the half-spaces of the geometric polytope $\mathfrak{D}^{g}_{1,1/1,3\text{-}1,2}$: see figures 2a and 2b.

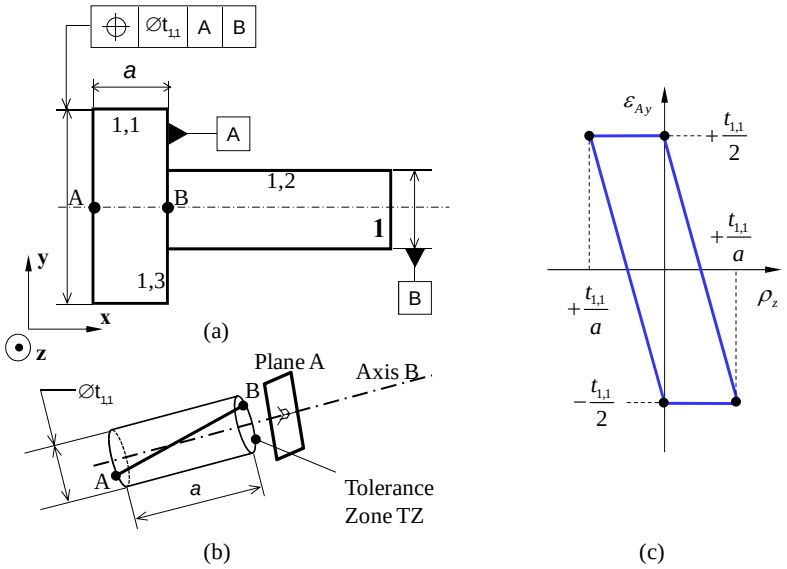

Figure 2: Localisation modelled by a geometric polytope.

The geometric polytope $\mathfrak{D}^{g}_{1,1/1,3\text{-}1,2}$ is defined by [1]:

$$\mathfrak{D}^{g}_{1,1/1,3-1,2} = \left\{ \forall N \in 1,1 : \boldsymbol{\varepsilon}_{N,1,1/1,3-1,2}.\mathbf{n}_N \le +\frac{t_{1,1}}{2} \right\} \text{ with } \mathbf{n}_N \text{ normal unit vector to 1,1 at point } N \quad (4)$$

$\boldsymbol{\varepsilon}_{N,1,1/1,3-1,2}$ is the translation vector of 1,1 with respect to 1,3-1,2 at point N .

As surface 1,1 is cylindrical, equation (4) can be written:

$$\mathfrak{D}^{g}_{1,1/1,3-1,2} = \left\{ \begin{array}{l} -\frac{t_{1,1}}{2} \le \boldsymbol{\varepsilon}_{A,1,1/1,3-1,2}.\mathbf{n}_{\boldsymbol{\theta}} \le +\frac{t_{1,1}}{2} \\ -\frac{t_{1,1}}{2} \le \boldsymbol{\varepsilon}_{B,1,1/1,3-1,2}.\mathbf{n}_{\boldsymbol{\theta}} \le +\frac{t_{1,1}}{2} \end{array} \right\} \quad (5)$$

$$\text{with: } \mathbf{n}_{\boldsymbol{\theta}} = \cos\theta.\mathbf{y} + \sin\theta.\mathbf{z} \left(i \in \mathbb{N} : \theta = i.\frac{\pi}{n}, 0 \le i < n \right)$$

According to the property of small displacement fields, this gives:

$$\forall N, M \left(\text{with } N \ne M\right) : \boldsymbol{\varepsilon}_{N,1,1/1,3-1,2} = \boldsymbol{\varepsilon}_{M,1,1/1,3-1,2} + \mathbf{NM} \times \boldsymbol{\rho}_{1,1/1,3-1,2} \quad (6)$$

$\boldsymbol{\rho}_{1,1/1,3-1,2}$ is the rotation vector of 1,1 with respect to 1,3-1,2.

Finally, $\mathfrak{D}^{g}_{1,1/1,3-1,2}$ is written at point A giving consideration to (5),(6):

$$\mathfrak{D}^{g}_{1,1/1,3-1,2}=\left\{\begin{array}{l}-\frac{t_{1,1}}{2}\le \boldsymbol{\varepsilon}_{\mathrm{A},1,1/1,3-1,2}.\mathbf{n}_{\boldsymbol{\theta}}\le+\frac{t_{1,1}}{2}\\ -\frac{t_{1,1}}{2}\le \left(\boldsymbol{\varepsilon}_{\mathrm{A},1,1/1,3-1,2}+\mathbf{BA}\times\boldsymbol{\rho}_{1,1/1,3-1,2}\right).\mathbf{n}_{\boldsymbol{\theta}}\le+\frac{t_{1,1}}{2}\end{array}\right\} \quad (7)$$

$$\text{with : } \mathbf{n}_{\boldsymbol{\theta}}=\cos\theta.\mathbf{y}+\sin\theta.\mathbf{z}\left(i\in\mathbb{N}:\theta=i.\frac{\pi}{n},0\le i<n\right)$$

Figure 2c shows a graphic representation of $\mathfrak{D}^{g}_{1,1/1,3-1,2}$, the 4d polytope defined in (7), projected in $\mathbb{R}^2$. The translation deviations at point A following $\mathbf{y}$ are projected onto axis ε_{Ay} and the rotation deviations following $\mathbf{z}$ are projected following ρ_z. The interior of the polytope (boundary included) represents the geometric deviations that comply with the location specification in figure 2a. The definition of the geometric polytope $\mathfrak{D}^{g}_{2,1/2,3-2,2}$ defining the location of part 2 is analogous with that of $\mathfrak{D}^{g}_{1,1/1,3-1,2}$.

The definition of a contact polytope characterising a contact specification is deduced from non-interference strains from which all the half-spaces of the contact polytope $\mathfrak{D}^{c}_{1,2/2,2}$ can be defined: see figure 3a.

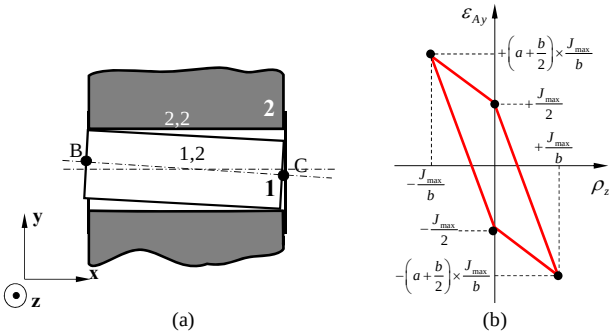

Figure 3: Cylinder pair contact modelled by a contact polytope.

Polytope $\mathfrak{D}^{c}_{1,2/2,2}$ is defined as:

$$\mathfrak{D}^{c}_{1,2/2,2}=\left\{\forall N\in 1,2:\boldsymbol{\varepsilon}_{N,1,2/2,2}.\mathbf{n}_{N}\le d_{N}\right\} \text{ with } \mathbf{n}_{N} \text{ normal unit vector to 1,1 at point } N \quad (8)$$

$\boldsymbol{\varepsilon}_{N,1,2/2,2}$ is the translation vector of 1,2 with respect to 2,2 at point N. d_N is the local distance in N between the two surfaces potentially in contact following $\mathbf{n}_{\mathrm{N}}$ in the specific position where the situation deviations between the two surfaces are null. In the example, the distance d_N is defined as a function of clearance J between surfaces 1,2 and 2,2:

$$d_{N}=\frac{J}{2} \quad (9)$$

As this is a cylindrical pair contact, equation (8) can be written:

$$\mathfrak{D}^{c}_{1,2/2,2}=\left\{\begin{array}{l}\boldsymbol{\varepsilon}_{\mathrm{B},1,2/2,2}.\mathbf{n}_{\boldsymbol{\theta}}\le+\frac{J}{2}\\ \boldsymbol{\varepsilon}_{\mathrm{C},1,2/2,2}.\mathbf{n}_{\boldsymbol{\theta}}\le+\frac{J}{2}\end{array}\right\} \quad (10)$$

$$\text{with: } \mathbf{n}_{\boldsymbol{\theta}}=\cos\theta.\mathbf{y}+\sin\theta.\mathbf{z}\left(i\in\mathbb{N}:\theta=i.\frac{2\pi}{n},0\le i<n\right)$$

Using the property of small displacement fields defined in (6), in the same way as polytope $\mathfrak{D}^{g}_{1,1/1,3-1,2}$, $\mathfrak{D}^{c}_{1,2/2,2}$ can be written at point A (see figure 3):

$$\mathfrak{D}^{c}_{1,2/2,2} = \left\{ \begin{array}{l} \left(\boldsymbol{\varepsilon}_{A,1,2/2,2} + \mathbf{BA} \times \boldsymbol{\rho}_{1,2/2,2}\right).\mathbf{n}_{\theta} \le +\dfrac{J}{2} \\ \left(\boldsymbol{\varepsilon}_{A,1,2/2,2} + \mathbf{CA} \times \boldsymbol{\rho}_{1,2/2,2}\right).\mathbf{n}_{\theta} \le +\dfrac{J}{2} \end{array} \right\} \tag{11}$$

with: $\mathbf{n}_{\theta} = \cos\theta.\mathbf{y} + \sin\theta.\mathbf{z} \left(i \in \mathbb{N} : \theta = i.\dfrac{2\pi}{n}, 0 \le i < n \right)$

$\boldsymbol{\rho}_{1,2/2,2}$ is the rotation vector of 1,2 with respect to 2,2 at point N. Figure 3b shows a graphic representation of $\mathfrak{D}^{c}_{1,2/2,2}$, 4d polytope defined by (11) in the configuration where $J = J_{\max}$ (i.e. the most unfavourable configuration for the FC), projected in $\mathbb{R}^2$. We then have (see figures 1c and 1d):

$$J_{\max} = \left(D_{2,2n} + d_{2,2\sup}\right) - \left(D_{1,2n} + d_{1,2\inf}\right) \tag{12}$$

The translation deviations at point A following $\mathbf{y}$ are projected onto axis ε_{Ay} and the rotation deviations following $\mathbf{z}$ are projected following ρ_z.

Figure 4a shows how polytope $\mathfrak{D}_{1,1/2,1}$ is determined from equation (3) projecting into $\mathbb{R}^2$ in the configuration where $J = J_{\max}$. Figure 4b shows in $\mathbb{R}^2$ that the FC is respected, in that the calculated polytope $\mathfrak{D}_{1,1/2,1}$ (2-dimension) must be contained inside the functional polytope $\mathfrak{D}^{f}_{1,1/2,1}$ (1-dimension). The following equations, characterising compliance with the FC, have therefore been deduced:

$$\left\{ \begin{array}{l} +\dfrac{J_{\max}}{2} + \dfrac{t_{1,1}}{2} + \dfrac{t_{2,1}}{2} \le +\mathrm{e}_{\max} \\ +\mathrm{e}_{\min} \le -\dfrac{J_{\max}}{2} - \dfrac{t_{1,1}}{2} - \dfrac{t_{2,1}}{2} \end{array} \right. \tag{13}$$

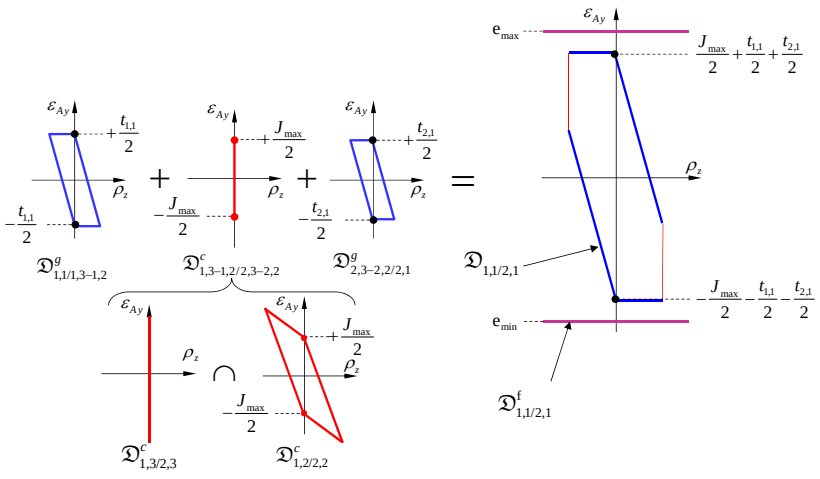

Figure 4: Respect of a functional condition by operations on polytopes in rigid behaviour.

2.2. Variability due to thermomechanical behaviour

Several studies have been carried out to manage compliant structure: [22], [23], [24], [25]. These take into account geometric variations induced by the assembly process and

manufacturing dispersions. Mandil et al. show the usefulness of considering functional requirement variations throughout the various phases of the product life cycle, by taking thermomechanical phenomena into account [26]. Simulation of the thermomechanical behaviour of the system studied is based on finite element digital simulations. Benichou et al. present a tolerance analysis method taking into account thermal dilatation, but this work does not integrate thermomechanical deviations of parts dependent on contact conditions with other parts [27]. The model produced in this article is based on a reference behaviour described in the preceding paragraph, with the system modelled using infinitely rigid parts. Each thermomechanical behaviour is characterised by a change in the reference behaviour.

The following hypotheses are postulated for each thermomechanical behaviour:

- invariance of the topological structure of the (contact) graph,
- variations in the form and dimensions of the parts are taken into account,
- no local strain on surfaces in contact.

The invariance of the topological structure of the graph means that there is no additional contact and no suppression of contact between two behaviours. In addition, each contact type remains the same: a cylindrical pair remains a cylindrical pair, a planar pair remains a planar pair, etc. However, the different parameters that define contact (minimal clearance, maximal clearance, nature of contact, ...) may change.

The thermomechanical behaviour of the system is presumed to be elastic; it is modelled in small strains and small displacements.

Let us consider figure 5a which shows a thermomechanical change in our system. For each part, a thermomechanical simulation by finite elements is carried out in a free state. The purpose of a simulation is to determine geometric variations of thermomechanical origin in a part, while considering no contact stress with the surrounding parts, and thus determine changes in contacts between parts.

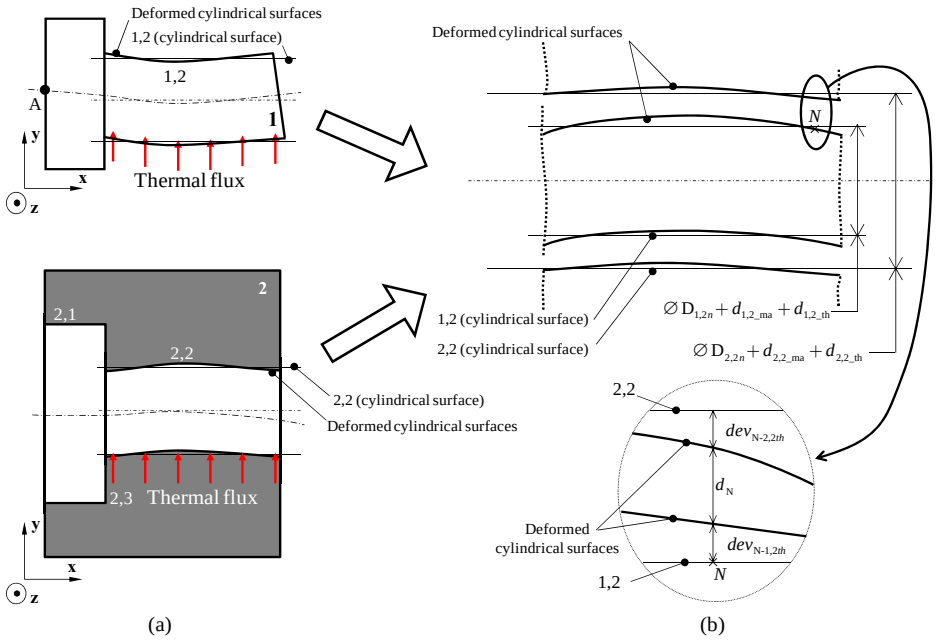

Figure 5: Geometric deviations between two deformed surfaces potentially in contact.

A method commonly used in 3d metrology will enable us to assess the geometric variations of thermomechanical origin in a part in a free state. A part under strain is modelled by a finite number of points, each one corresponding to a node in the mesh of this part. An ideal surface (plane, cylinder, cone, ...) is associated to the mesh nodes using the least squares criterion.

Thus the cylindrical surfaces 1,2 and 2,2 are associated to the nodes of strains on two nominal cylindrical surfaces.
Simulation of a joint between two parts that are potentially in contact consists of determining the contact polytope in the event that the surfaces in contact are under thermomechanical strain. The condition of non-interpenetration defined in (8) no longer depends solely on clearance between the two surfaces due to manufacturing deviations but also on local clearance due to dimension and form deviations of thermomechanical origin. Local clearance d_{N} at point N is defined as a function of clearance J between the two substituted surfaces 1,2 and 2,2 and as a function of form deviations of thermomechanical origin $dev_{\mathrm{N\text{-}1,2-}th}$ and $dev_{\mathrm{N\text{-}2,2-}th}$ in surfaces 1,2 and 2,2 respectively (see figure 5b) :

$$d_{\mathrm{N}} = \frac{J}{2} + \left(dev_{\mathrm{N\text{-}2,2-}th} - dev_{\mathrm{N\text{-}1,2-}th} \right) \tag{14}$$

In this case, clearance J between the two substituted surfaces is defined in the following:

$$J = \mathrm{D}_{2,2} - \mathrm{D}_{1,2} = \left(\mathrm{D}_{2,2n} + d_{2,2\_\mathrm{ma}} + d_{2,2\_\mathrm{th}} \right) - \left(\mathrm{D}_{1,2n} + d_{1,2\_\mathrm{ma}} + d_{1,2\_\mathrm{th}} \right)$$

with:

$\mathrm{D}_{1,2n}, \mathrm{D}_{2,2n}$: nominal diameters (15)

$d_{1,2\_\mathrm{ma}}, d_{2,2\_\mathrm{ma}}$: diameter deviation du to manufacturing process

$d_{1,2\_\mathrm{th}}, d_{2,2\_\mathrm{th}}$: diameter deviation du to thermomechanical strains

The least favourable configuration for the FC in relation to manufacturing deviations is that which corresponds to:

$$J_{\max} = \left(\mathrm{D}_{2,2n} + d_{2,2\mathrm{sup}} + d_{2,2\_\mathrm{th}} \right) - \left(\mathrm{D}_{1,2n} + d_{1,2\mathrm{inf}} + d_{1,2\_\mathrm{th}} \right) \tag{16}$$

Finally, for the CP joint in its least favourable configuration, equation (8) is written at point A:
$\forall N \in 1,2$

$$\left\{ \left(\boldsymbol{\varepsilon}_{A\text{–}1,2/2,2} + NA \times \boldsymbol{\rho}_{1,2/2,2} \right).\mathbf{n}_N \le \frac{J_{\max}}{2} + \left(dev_{\mathrm{N\text{-}2,2-}th} - dev_{\mathrm{N\text{-}1,2-}th} \right) \right\} \tag{17}$$

with: $\mathbf{n}_{\boldsymbol{\theta}} = \cos\theta.\mathbf{y} + \sin\theta.\mathbf{z} \left(i \in \mathbb{N} : \theta = i.\frac{2\pi}{n}, 0 \le i < n \right)$

The polytope defined in (17) is generally expressed $\mathfrak{D}^{\mathrm{c,th}}_{1,2/2,2}$. There are two possibilities:

- (a) the intersection between the half-spaces defined by (17) generates a polytope,
- (b) the intersection between the half-spaces defined by (17) generates an empty set.

Case (a) is illustrated in figure 6 where the polytope $\mathfrak{D}^{\mathrm{c,th}}_{1,2/2,2}$, represented in two specific projection planes, defines the relative positions of surfaces 1,2 and 2,2 at point A.

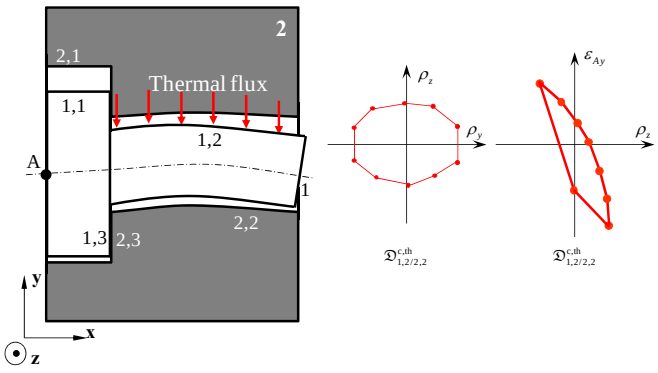

Figure 6: Contact polytope between two deformed surfaces without clamping.

Case (b) corresponds to a local clamping phenomenon, also called local tightening, between the two parts. No movement between the two surfaces relative to one another is possible: the specifications state that the joint has fixed contact. The contact polytope $\mathfrak{D}^{c,th}_{1,2/2,2}$ is a vertex that coincides with the origin: see figure 7.

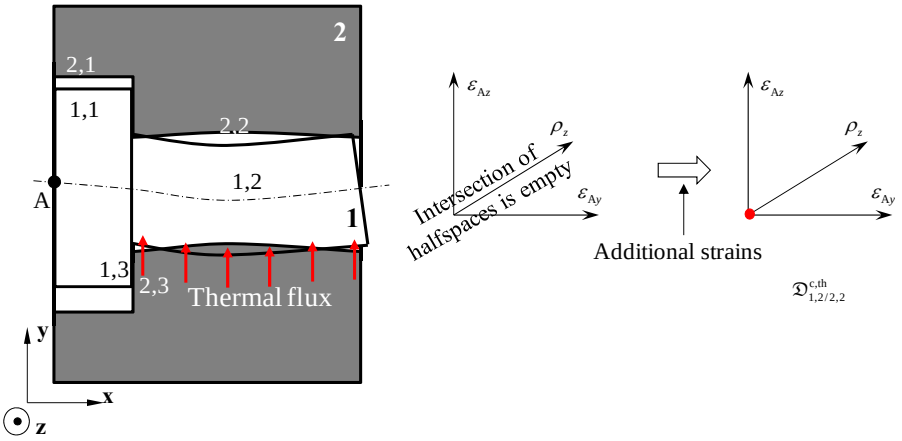

Figure 7: Contact polytope between two deformed surfaces with clamping.

Let us consider the functional condition defined in equation (1) characterised by the functional polytope $\mathfrak{D}^{f}_{1,1/2,1}$. Equation (3), which defines respect of the functional condition, remains the same, given that the topological structure of the system between one thermomechanical behaviour and the reference behaviour is presumed to be invariant.
A thermomechanical study of the complete system has to be carried out so as to take into account the contact conditions between the parts in the thermomechanical behaviour. The clamping or non-clamping phenomena are modelled in the contact limit conditions between parts using finite element modelling. Figure 8 shows the result from a thermomechanical calculation on the complete system.

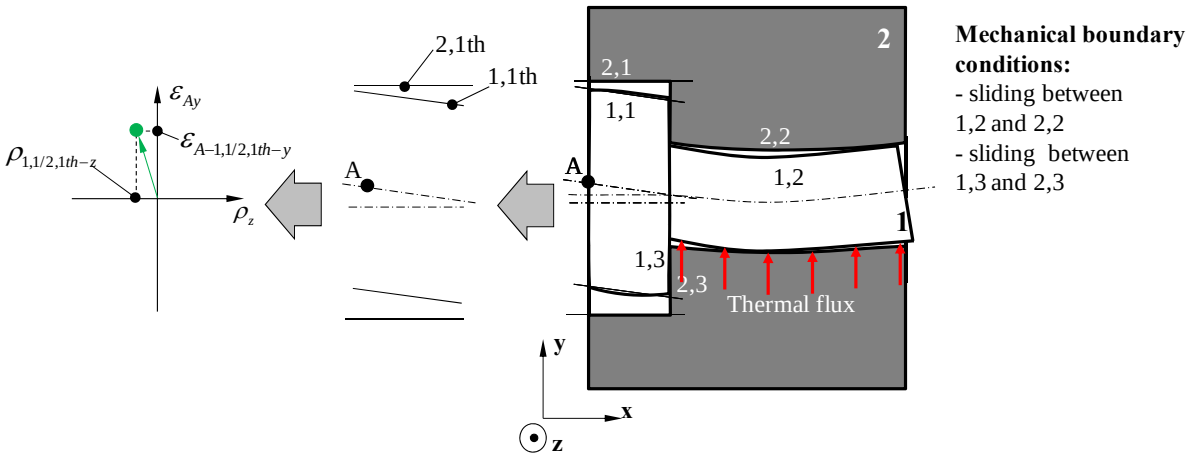

Figure 8: Characterisation of the thermomechanical behaviour of the complete system.

The aim of the thermomechanical simulation is to define the polytope $\mathfrak{D}^{th}_{1,1/2,1}$ with which it will be possible to determine deviations of thermomechanical origin between surfaces 1,1 and 2,1. The same method is used here as was used previously to determine deviations of thermomechanical origin on a part under stress in a free state: see figure 8.

From (3), equation (18) defines determining polytope $\mathfrak{D}_{1,1/2,1}$ with:

- $\mathfrak{D}^{th}_{1,1/2,1}$: polytope characterising deviations of thermomechanical origin between surfaces 1,1 and 2,1,
- $\mathfrak{D}^{g}_{1,1/1,3\text{-}1,2}$, $\mathfrak{D}^{g}_{2,3-2,2/2,1}$: geometric polytopes characterising geometric variations limited by the location specifications,
- $\mathfrak{D}^{c,th}_{1,2/2,2}, \mathfrak{D}^{c,th}_{1,3/2,3}$: contact polytopes characterising geometric variations induced by diameter specifications and the thermomechanical behaviour of the parts.

We thus obtain:

$$\mathfrak{D}_{1,1/2,1} = \mathfrak{D}^{th}_{1,1/2,1} + \mathfrak{D}^{g}_{1,1/1,3\text{-}1,2} + \left(\mathfrak{D}^{c,th}_{1,2/2,2} \cap \mathfrak{D}^{c,th}_{1,3/2,3}\right) + \mathfrak{D}^{g}_{2,3-2,2/2,1} \tag{18}$$

Figure 9a shows the construction of the polytope $\mathfrak{D}_{1,1/2,1}$ defined by equation (18). The inclusion of the calculated polytope in the functional polytope shown in figure 9b characterises compliance with the functional condition. It therefore follows:

$$\begin{cases} +\frac{t_{1,1}}{2} + +\frac{t_{2,1}}{2} + \varepsilon_{A-1,1/2,1th\text{-}y} \le +\mathrm{e}_{\max} \\ +\mathrm{e}_{\min} \le -\frac{t_{1,1}}{2} - \frac{t_{2,1}}{2} + \varepsilon_{A-1,1/2,1th\text{-}y} \end{cases} \tag{19}$$

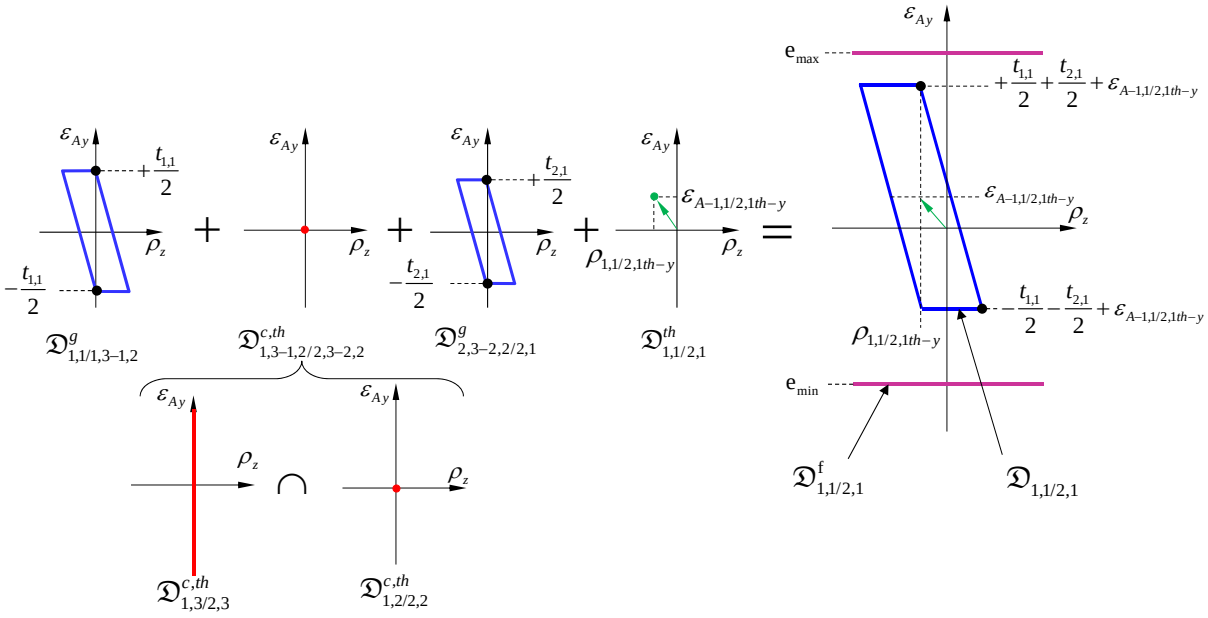

Figure 9: Respect of a functional condition by operations on polytopes in thermomechanical behaviour.

3. Turbine performance criteria

In this part we define the relationship between two performance criteria (energy yield and risk of the blades touching the stator) and the geometric variability of a turbine stator. The different turbine architectures that will be analysed in relation to the two performance criteria in §4 will all have the same rotor. We hypothesise that the geometric variability of the rotor will not be discriminant in this example. This variability will therefore not be described in detail.

3.1. *Correlation of performance criteria with geometrical criteria*

The correct functioning of a turbine relies on two performance criteria: energy yield and the risk of the blades touching the stator. These two performance criteria depend on the clearance between the turbine blades and the stator. Turbine energy yield is correlated with the flow of gas between the blade tips and the stator. This flow rate depends on the leakage section, the difference between the rotor and the stator sections; in order to guarantee optimal yield, it must not exceed a maximal value: $S_{\max}$.

To maximise the turbine's energy yield, rotor-stator clearance should be as small as possible while ensuring that in all of the turbine's operational phases the blades are not too close to the stator (which could damage the turbine and risk damaging the engine in operation). The risk of touching is correlated with a minimal clearance value that must be respected: $C_{\min}$.

3.2. *Geometrical criteria*

Local clearance between the blades and the stator $C(\theta)$ should be sufficient to avoid touching any part of the periphery of the turbine (see figure 10).

The touch criterion can be expressed by the following equation, where $C_{\min}$ is the minimum clearance that guarantees that the turbine functions correctly.

$$C(\theta) > C_{min} \quad \theta \in [0; 2\pi[\tag{20}$$

The leaking of gas between the stator and the rotor is determined by the leakage section S (see figure 10).

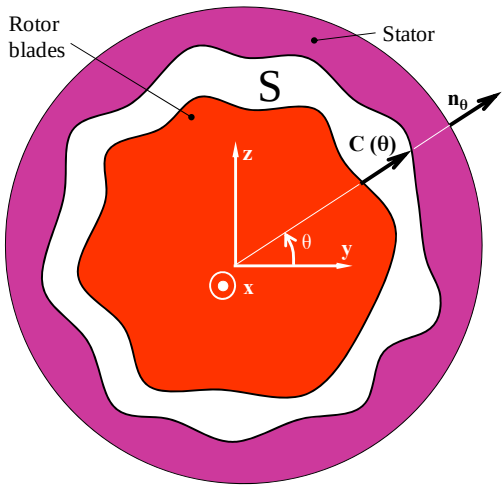

Figure 10: Sections of rotor blades and stator.

The criterion for power in a turbine is correlated with the leakage section. To maximise turbine power the leakage section must be minimised, as defined in the following equation:

$$S < S_{\max} \quad \text{with } S = S_{stator} - S_{rotor} \tag{21}$$

S_{stator} defines the section of the ring that is close up to the rotor, with the section of the rotor expressed as S_{rotor} .

3.3. *Stator variability*

$\boldsymbol{\delta}_{stator}(M, \theta)$ defines the position of a point on the real profile, with M the centre of the least squares circle and according to angle θ, in relation to the reference axis (figure 11). The

reference axis is the nominal axis of the stator, which coincides with the nominal axis of the rotor.

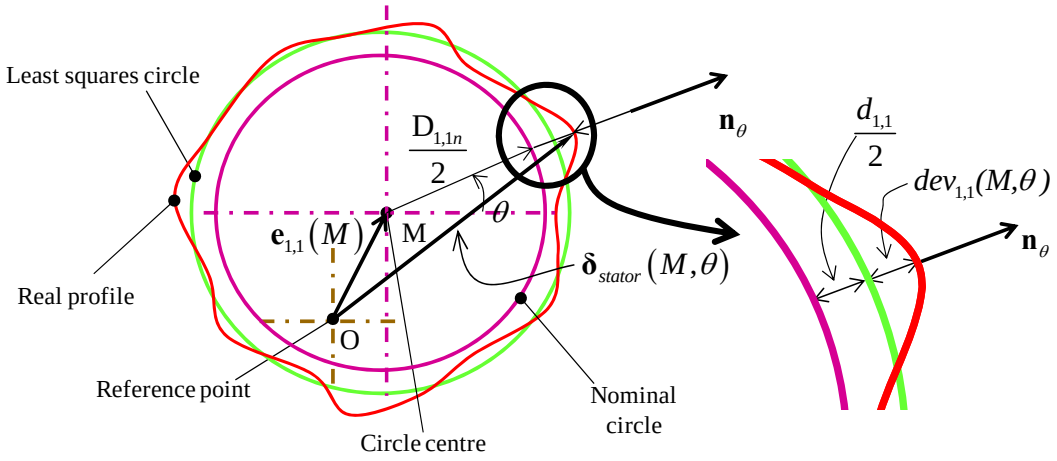

Figure 11: Parameters of a nominal circular surface.

The position $\boldsymbol{\delta}_{stator}(M,\theta)$ is written:

$$\boldsymbol{\delta}_{stator}(M,\theta) = \mathbf{e}_{1,1}(M) + \left(\frac{D_{1,1n}}{2} + \frac{d_{1,1}}{2} + dev_{1,1}(M,\theta) \right).\mathbf{n}_\theta \quad (22)$$

The preceding equation is defined as follows:

- $\mathbf{e}_{1,1}(M)$: location deviation of the centre of the substitute circle in relation to the reference axis,
- $D_{1,1n}$: nominal diameter,
- $d_{1,1}$: dimension deviation between the nominal diameter and the substitute circle diameter,
- $dev_{1,1}(M,\theta)$: form deviation of the real profile in relation to the substitute circle.

In the same way, $\boldsymbol{\delta}_{rotor}(M,\theta)$ defines the position of a point located on the profile of the real rotor at the tip of the blades.

By integrating equation (22) into equation (20), the touch criterion can be defined as follows:

$$\mathbf{C}(\theta) = \mathbf{e}_{1,1}(M) + \left(\frac{D_{1,1n}}{2} + \frac{d_{1,1}}{2} + dev_{1,1}(M,\theta) \right).\mathbf{n}_\theta - \boldsymbol{\delta}_{rotor}(M,\theta) \text{ with : } \theta \in [0;2\pi[\quad (23)$$

By combining equation (22) with equation (21), which describes the stator, the energy yield criterion is then defined as:

$$S = \int_0^{2\pi} \frac{1}{2}.\left(\frac{D_{1,1n}}{2} + \frac{d_{1,1}}{2} + dev_{1,1}(M,\theta) \right)^2 .d\theta - S_{rotor} \quad (24)$$

The deviations in dimension and shape are very small compared with the nominal diameter of the stator section. The integral which formalises the area of the stator section in equation (24) can then be linearised:

$$S_{stator} = \pi \times \left(\frac{D_{1,1n}}{2} \right)^2 + \frac{D_{1,1n}}{2} \times \int_0^{2\pi} \left(\frac{d_{1,1}}{2} + dev_{1,1}(M,\theta) \right).d\theta \quad (25)$$

4. Application to a simplified turbine model

4.1. Description of the simplified turbine

The simplified turbine model (figure 12) consists of two sub-units: a stator (parts labelled 1 and 2) and a rotor (part labelled 3), with a turning pair contact around **x** : see figure 12. Part 3 forms a revolution, where the largest diameter corresponds to the diameter of the blade tips.

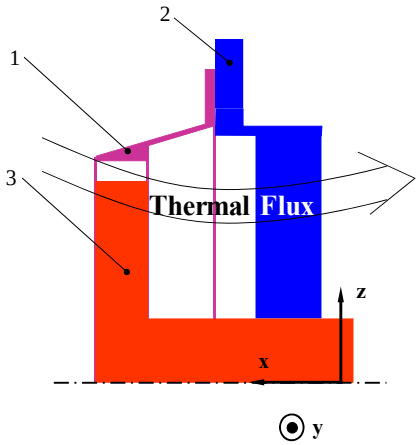

Figure 12: Simplified geometric model of a turbine.

When the engine is in operation, a flow of hot gases (1000°C approx.) is created by the combustion chamber (not shown in figure 12) and as a result parts 1, 2 and 3 undergo strain. In this example, only the thermomechanical strains on part 1 are taken into account when the engine is in operation.

In the following part of the article, parts 2 and 3 are assumed to be infinitely rigid and geometrically perfect. Moreover, the turning pair contact between part 2 and part 3 is considered to have no defects and no clearance.

The criteria defined in §3 will be studied for two different turbine architectures. Two variants of a technical solution will be considered, the aim being to produce a clamping contact between part 1 and part 2 (see figures 13 and 14):

- Architecture 1: planar pair contact with five short centring plugs located on a diameter D and distributed equiangularly.
- Architecture 2: planar pair contact with one short centring plug.

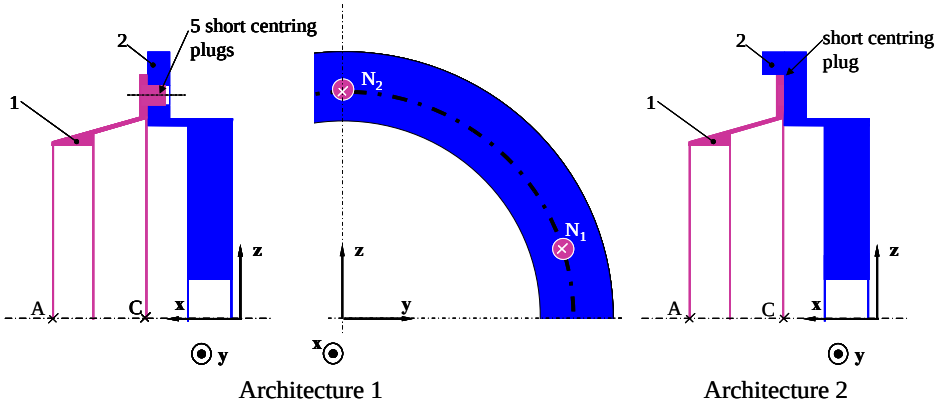

Figure 13: Turbine architectures.

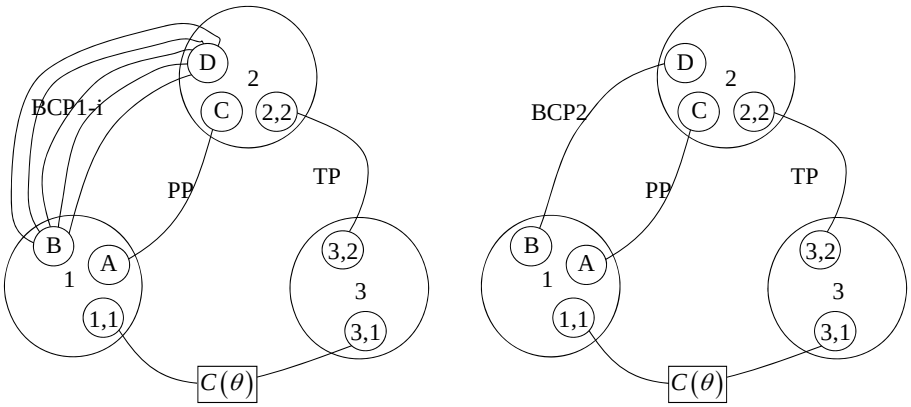

Architecture 1 **Architecture 2**

Features of BCP1-i (1 ≤ i ≤ 5) between 1,i and 2,i:

-Type : Ball and Cylinder Pair (BCP)

-Situation element : point Ni, line (Ni, x)

-Nature : floatting contact

-Clearance : 0 ≤ Jmin ≤ Jmax

Features of PP between 1,7 and 2,7:

-Type : Planar Pair (PP)

-Situation element : line (C, x)

-Nature : sliding contact

-Clearance : Jmax =Jmin = 0

Features of BCP2 between 1,1 and 2,1:

-Type : Ball and Cylinder Pair (BCP)

-Situation element : point C, line (C, x)

-Nature : floatting contact

-Clearance : Jmax =Jmin = 0

Features of TP between 1,7 and 2,7:

-Type : Planar Pair (PP)

-Situation element : line (C, x)

-Nature : sliding contact

-Clearance : Jmax =Jmin = 0

Figure 14 : Graph representations.

4.2. Defining parameters and formulating performance criteria

According to the hypotheses defined in the previous paragraph, the geometric variabilities of the two technical solutions considered depend only on the processes of obtaining part 1, and assembling parts 1 and 2 together, and the thermomechanical behaviour of part 1.

Equation (23) defines the touch criterion; this then becomes:

$$C(\theta) = \Delta C(\theta) + C_0$$

with :

$$\Delta C(\theta) = \mathbf{e}_{1,1}(M).\mathbf{n}_\theta + \frac{d_{1,1}}{2} + dev_{1,1}(M,\theta) \tag{26}$$

$$C_0 = \frac{\mathrm{D}_{1,1n}}{2} - \boldsymbol{\delta}_{rotor}(M,\theta).\mathbf{n}_\theta$$

Equation (24) defining the energy yield criterion then becomes:

$$S = \Delta S + S_0$$

with:

$$\Delta S = \frac{\mathrm{D}_{1,1n}}{2} \times \int_0^{2\pi} \left(\frac{d_{1,1}}{2} + dev_{1,1}(M,\theta) \right) .d\theta \tag{27}$$

$$S_0 = \pi \times \left(\frac{\mathrm{D}_{1,1n}}{2} \right)^2 - S_{rotor}$$

$\Delta C(\theta)$ and ΔS are dependent on the architecture variants. C_0 and S_0 are variables that are independent of the architectures by hypothesis.

4.3. Geometric characterisation

In the first phase, the turbine is modelled in a reference behaviour where all the solids are infinitely rigid: only manufacturing defects and clearance in the different contacts is taken into account. In phase two, a thermomechanical behaviour is considered, where there are strains due to the flow of hot gases from the combustion chamber at a point when the turbine is operating in a steady regime. Thermomechanical strains are then integrated into the reference model as described in §2.2.

4.3.1. Characterisation of the variability of production and assembly processes

Figures 13 and 14 describe the two architectures considered.
For architecture 1, clamping contact consists of a planar pair contact and five ball and cylinder pair contacts, with clearance, by means of five centring slugs. For architecture 2, clamping contact consists of a planar pair contact and one ball and cylinder pair contact, with a clamping screw.
In both architectures, bolts are used to keep parts 1 and 2 in position. They are not considered in the modelling process as they do not affect the relative positioning of parts 1 and 2.
Determination of: $e_{1,1/3,1}(M) = \mathbf{e}_{1,1/3,1}(M).\mathbf{n}_\theta$ is based on a 3d dimension chain formalised by operations on the polytopes (intersections and Minkowski sums).
The polytope that defines the displacement limits of surface 1,1 in relation to surface 3,1 is expressed by the following Minkowski sum:

$$\mathfrak{D}_{1,1/3,1} = \mathfrak{D}^g_{1,1/AB} + \mathfrak{D}^c_{AB/CD} + \mathfrak{D}^g_{CD/2,2} + \mathfrak{D}^c_{2,2/3,2} + \mathfrak{D}^g_{3,2/3,1} \quad (28)$$

$\mathfrak{D}^c_{AB/CD}$ is the contact polytope defined by the planar pair contact and the five ball and cylinder pair contacts for architecture 1 and the one ball and cylinder pair contact for architecture 2. $\mathfrak{D}^g_{1,1/AB}$ is the geometric polytope characterised by the location of surface 1,1 in relation to reference system AB according to ISO standards [19], [20] and [21] for the two architectures (see figure 15).

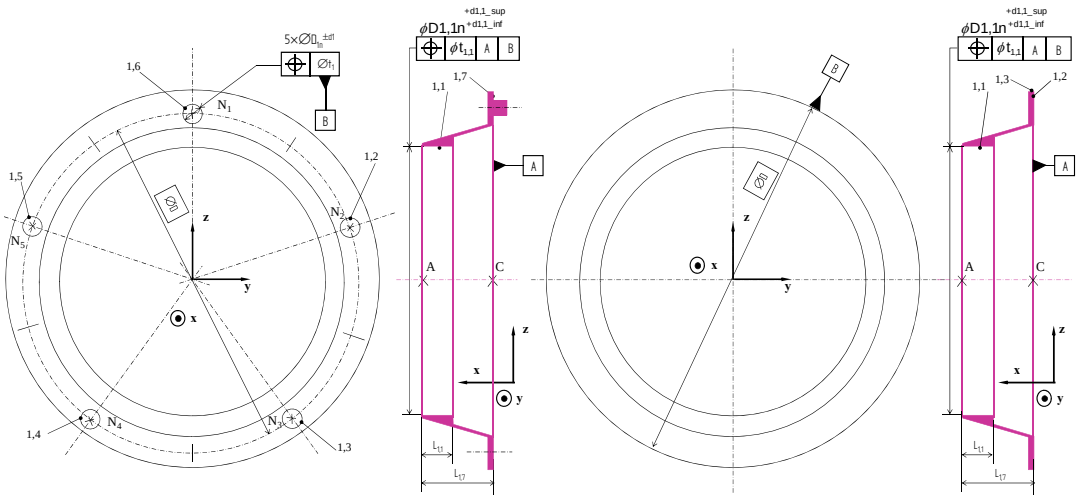

Architecture 1 Architecture 2

Figure 15: Definitions of parts 1.

Polytopes $\mathfrak{D}^{g}_{CD/2,2}$ and $\mathfrak{D}^{g}_{3,2/3,1}$ characterise the geometric polytopes for parts 2 and 3 respectively, and polytope $\mathfrak{D}^{c}_{2,2/3,2}$ characterises the contact polytope for the turning pair contact between parts 2 and 3.

According to the hypotheses advanced in §4.1, equation (9) then becomes:

$$\mathfrak{D}_{1,1/3,1} = \mathfrak{D}^{g}_{1,1/AB} + \mathfrak{D}^{c}_{AB/CD} \tag{29}$$

The calculated polytopes $\mathfrak{D}_{1,1/3,1}$ resulting from the Minkowski sums defined by equation (29) are shown in figure 16, where $J_{\max}$ represents clearance in the five ball and cylinder pair contacts and $t_{1,1}$ the dimension of the tolerance zone for the location specification of surface 1,1.

From figure 16 we can determine the values of the location deviation between surfaces 1,1 and 3,1.

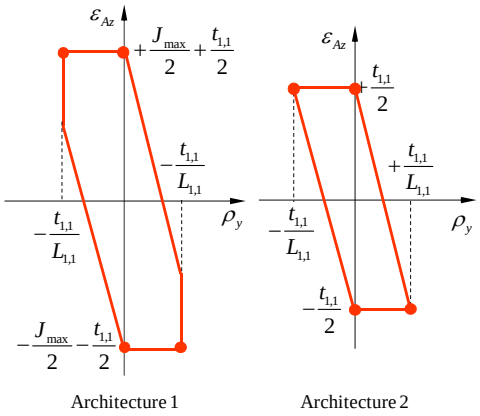

Figure 16: Geometric polytope of location of surface 1,1 at point A.

Equations (30) and (31) define the minimal and the maximal values of this deviation for architecture 1 and architecture 2 respectively:

$$-\frac{J_{\max}}{2}-\frac{t_{1,1}}{2} \le e_{1,1\_A1}(M) \le +\frac{J_{\max}}{2}+\frac{t_{1,1}}{2} \tag{30}$$

$$-\frac{t_{1,1}}{2} \le e_{1,1\_A2}(M) \le +\frac{t_{1,1}}{2} \tag{31}$$

As seen in the definition drawing for part 1, the dimension deviations for surface 1,1 in the two architectures are given in equations (32) and (33).

$$\mathrm{d}_{1,1\_inf} \le d_{1,1\_A1} \le \mathrm{d}_{1,1\_sup} \tag{32}$$

$$\mathrm{d}_{1,1\_inf} \le d_{1,1\_A2} \le \mathrm{d}_{1,1\_sup} \tag{33}$$

By definition, deviations in form due to manufacture are not taken into account, which gives:

$$dev_{1,1\_A1}(M,\theta) = dev_{1,1\_A2}(M,\theta) = 0 \tag{34}$$

4.3.2. Characterisation of thermomechanical variability

Thermomechanical strains caused by a flow of gases from the combustion chamber and illustrated in figure 17 have to be integrated into the geometric variability of the stator.

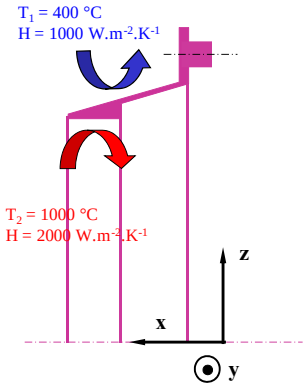

Figure 17: Thermal marginal conditions.

As described in §2.2, thermomechanical studies were made of different parts in the free state. This was to detect whether any clamping was present in the contacts. In this example, only part 1 was studied in the free state since parts 2 and 3 are considered to be infinitely rigid from the hypotheses formulated in §4.1. Thermomechanical calculations were made using Abaqus software.
In architecture 1, radial displacement of the slugs in their housing uses up all the clearance (see figure 18).

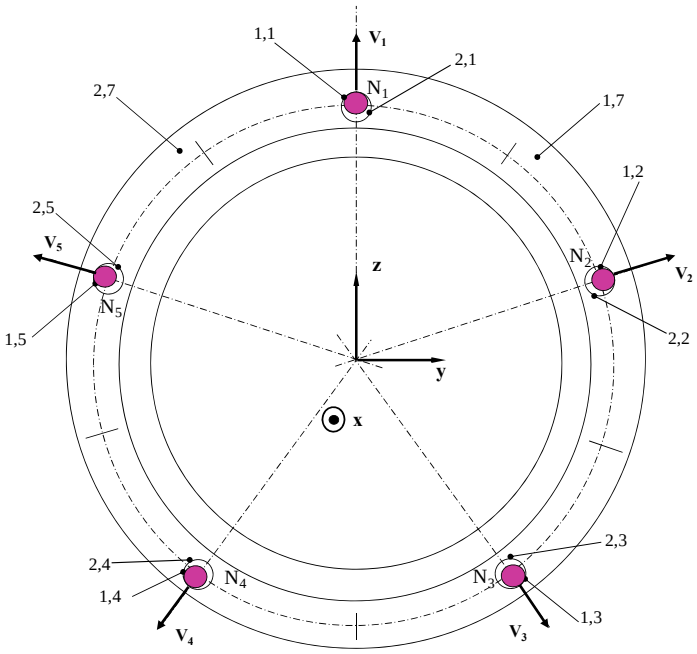

Figure 18: Radial displacements of the slugs.

This represents clamping between parts 1 and 2 with positioning by joints BCP1-i.
The planar pair contact / short centring used in the technical solution for architecture 2 remains without clearance, however, clamping caused by tightening of surface B on surface D appears in joint BCP2.
Lastly, in architecture 1, a thermomechanical analysis of part 1 was carried out using the thermal limit conditions defined in figure 17, the mechanical limit conditions defined in figure 14 and incorporating clamping in joints BCP1-i as shown in figure 18.
A similar thermomechanical analysis was carried out for architecture 2 with the same thermal limit and mechanical limit conditions and incorporating clamping in joint BCP2.
From these two thermomechanical analyses, strains in surface 1,8 could be characterised for architectures 1 and 2 in a plane section: see figure 19.

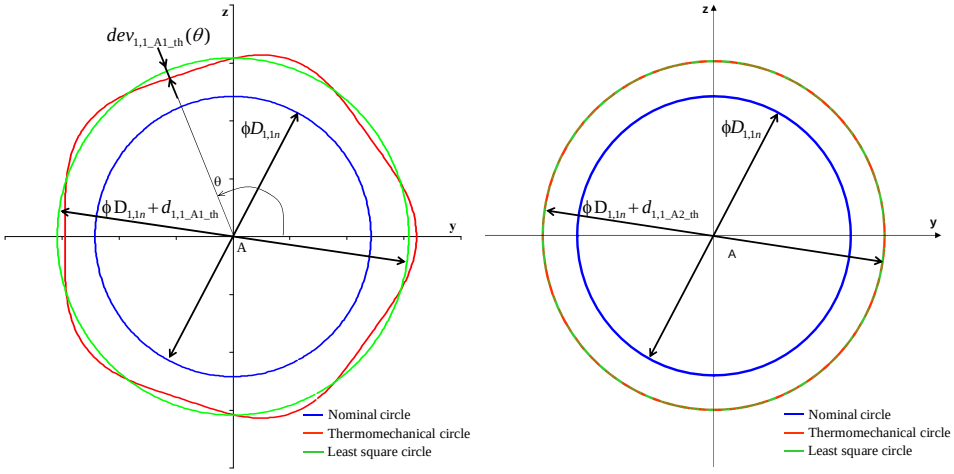

Architecture 1 Architecture 2

Figure 19: Thermomechanical strains of surface 1,1 in plane (A, ***x***).

From figure 19 we can determine location deviation, dimension deviation and form deviation, due to thermomechanical strain for both architectures.

When changes in contacts, changes in geometry, and the different deviations defined in equations (30) to (34) are incorporated, this gives:

$$-\frac{t_{1,1}}{2} \le e_{1,1\_A1}(M) \le +\frac{t_{1,1}}{2} \tag{35}$$

$$-\frac{t_{1,1}}{2} \le e_{1,1\_A2}(M) \le +\frac{t_{1,1}}{2} \tag{36}$$

$$\mathrm{d}_{1,1\_inf} + \mathrm{d}_{1,1\_A1\_th} \le d_{1,1\_A1} \le \mathrm{d}_{1,1\_sup} + \mathrm{d}_{1,1\_A1\_th} \tag{37}$$

$$\mathrm{d}_{1,1\_inf} + \mathrm{d}_{1,1\_A2\_th} \le d_{1,1\_A2} \le \mathrm{d}_{1,1\_sup} + \mathrm{d}_{1,1\_A2\_th} \tag{38}$$

$$\mathrm{dev}_{1,1\_A1\_th\_min} \le dev_{1,1\_A1}(M,\theta) \le \mathrm{dev}_{1,1\_A1\_th\_max} \tag{39}$$

$$dev_{1,1\_A2}(M,\theta) = 0 \tag{40}$$

4.4. Defining the two architectures

All the parameters defining the variability of clearance at the blade tips as a function of geometric and architectural variability have been defined. These different parameters are then exploited to compare the two architectures one with another in terms of thermomechanical situation.

From equations (41) and (42), for thermomechanical behaviour, we can compare variations in minimal clearance for the two architectures.

$$\left.\begin{aligned} &-\frac{t_{1,1}}{2} + \mathrm{d}_{1,1\_inf} + \mathrm{d}_{1,1\_A1\_th} \\ &+dev_{1,1\_A1\_th\_min} + C_0 \end{aligned}\right) > C_{min} \tag{41}$$

$$-\frac{t_{1,1}}{2} + \mathrm{d}_{1,1\_inf} + \mathrm{d}_{1,1\_A2\_th} + C_0 > C_{min} \tag{42}$$

From equations (43) and (44) we can compare the energy yield of the two architectures, from variations in the leakage sections.

$$\pi \times \mathrm{D}_{stator} \times \frac{\mathrm{d}_{1,1\_inf} + \mathrm{d}_{1,1\_A1\_th}}{2} + S_0 < S_{\max} \tag{43}$$

$$\pi \times D_{stator} \times \frac{d_{1,1\_inf} + d_{1,1\_A2\_th}}{2} + S_0 < S_{max} \quad (44)$$

To compare the two architectures in terms of thermomechanical behaviour, only dimension deviations and shape deviations are determinant in relation to the two performance criteria. Thermomechanical calculations give the following results:

$$d_{1,1\_A1\_th} < d_{1,1\_A2\_th} \text{ and } dev_{1,1\_A1\_th\_min} < 0 \quad (45)$$

Where the risk of touching predominates over energy yield, architecture 2 is the most efficient.

Where energy yield predominates over the risk of touching, then architecture 1 performs best.

Thus the preponderance of one or other of the two performance criteria determines which is the more efficient solution.

5. Conclusions-Future developments

The geometric variability described in this article is based on a variational approach formalised by operations on polytopes. This enables us to take into account the multiphysical behaviour of a mechanical system by incorporating variabilities inherent in processes relating to obtaining parts, assembly processes and the thermomechanical behaviour of the system, all in the same model.

With this model we were able to determine variations in rotor/stator clearance at the tips of the blades in the high pressure turbine of a turboshaft engine under two different behaviours: a reference behaviour (parts at 20°C) and a thermomechanical behaviour (combustion chamber at approximately 1000°C). The variations in rotor/stator clearance gave rise to two different turbine architectures in relation to two performance criteria: energy yield and the risk of touching the blade. This model can be used at a very early stage in the design cycle and will enable the designer to focus on turbine architecture at the architectural design phase.

Only two operational cycle behaviours are dealt with in this article, but there are several others that can be considered, especially in the most critical phases of turbine operation, such as starting up, for example. In addition, only two types of joint between the ring support and the turbine housing were analysed. In future work, other joints will be studied between different parts which could have different forms and dimensions, and in the near future, thermomechanical strains in several parts of the stator will be considered.

Finally, geometric variations resulting from residual strains from manufacturing processes (e.g. welding metal parts or RTM injection of parts made of composite materials) have an important role to play and will be incorporated into these studies.

6. References

[1] D. Teissandier, V. Delos, Operations on polytopes: application to tolerance analysis, in: Proc. of 6th CIRP Seminar on Computer Aided Tolerancing, ISBN 0-7923-5654-3, Enschede (Netherlands), 1999: p. 425–433.

[2] G. Ziegler, Lectures on polytopes, ISBN 0-387-94365-X, Springer Verlag, 1995.

[3] D. Teissandier, V. Delos, Algorithm to calculate the Minkowski sums of 3-polytopes based on normal fans, Computer-Aided Design. 43 (2011) 1567–1576.

[4] Y. Wu, J.J. Shah, J.K. Davidson, Improvements to algorithms for computing the Minkowski sum of 3-polytopes, Computer-Aided Design. 35 (2003) 1181–1192.

[5] A. Ballu, L. Mathieu, O. Legoff, Representation of Mechanical Assemblies and Specifications by Graphs, in: Geometric tolerancing of products, ISBN 978-1-84821-118-6, ISTE-WILEY, 2010: p. 87–110.

[6] M. Giordano, D. Duret, Clearance Space and Deviation Space, in: Proc. of 3rd CIRP seminar on Computer Aided Tolerancing, ISBN 2-212-08779-9, Cachan (France), 1993: p. 179–196.

[7] J.K. Davidson, A. Mujezinovic, J.J. Shah, A new mathematical model for geometric tolerances as applied to round faces, ASME Transactions on Journal of Mechanical Design. 124 (2002) 609–622.
[8] U. Roy, B. Li, Representation and interpretation of geometric tolerances for polyhedral objects. II.: Size, orientation and position tolerances, Computer-Aided Design. 31 (1999) 273–285.
[9] L. Pierre, D. Teissandier, J.P. Nadeau, Integration of thermomechanical strains into tolerancing analysis, International Journal on Interactive Design and Manufacturing. 3 (2009) 247–263.
[10] L. Pierre, D. Teissandier, J.-P. Nadeau, Integration of multiple physical behaviours into a geometric tolerancing approach, in: Proc. of 11th CIRP Seminar on Computer Aided Tolerancing, in CDRom, Annecy (France), 2009.
[11] M. Giordano, S. Samper, J. Petit, Tolerance analysis and synthesis by means of deviation domains, axi-symmetric cases, in: ISBN 978-1-4020-5437-2, Springer, Tempe (Arizona - USA), 2007: p. 85–94.
[12] A. Mujezinovic, J.K. Davidson, J.J. Shah, A new mathematical model for geometric tolerances as applied to polygonal faces, ASME Transactions on Journal of Mechanical Design. 126 (2004) 504–518.
[13] T.L. Defazio, A.C. Edsall, R.E. Gustavson, J. Hernandez, P.M. Hutchins, H.W. Leung, et al., A prototype of feature based design for assembly, Journal of Mechanical Design. 115 (1993) 723–734.
[14] D.E. Whitney, J.D. Adams, Application of screw theory to analysis of mobility and constraint of mechanisms, Journal of Mechanical Design. 123 (2001) 26–32.
[15] J.Y. Dantan, L. Mathieu, A. Ballu, P. Martin, Tolerance synthesis: quantifier notion and virtual boundary, Computer-Aided Design. 37 (2005) 231–240.
[16] J. Dufaure, D. Teissandier, A tolerancing framework to support geometric specifications traceability, International Journal of Advanced Manufacturing Technology. 36 (2008) 894–907.
[17] ISO3952-1, Kinematic diagrams - Graphical symbols-Part 1, (1981).
[18] D. Teissandier, J. Dufaure, Product Model for Tolerancing, in: Geometric tolerancing of products, ISBN 978-1-84821-118-6, ISTE-WILEY, 2010: p. 55–86.
[19] ISO8015, Technical drawings - Fundamental tolerancing principle, (1985).
[20] ISO1101, Geometrical Product Specifications (GPS), Geometrical tolerancing, Tolerances of form, orientation, location and run-out, (2004).
[21] ISO5459, Technical drawings - Geometrical tolerancing - Datums and datum-systems for geometrical tolerances, (1981).
[22] J.S. Hu, J. Camelio, Modeling and control compliant assembly systems, Annals of the CIRP Manuf. Technol. 55 (2006) 19–22.
[23] M.L. Stewart, K.W. Chase, Variation simulation of fixtured assembly for compliant structures using piecewise-linear analysis, in: Proc. of ASME IMECE2005-82371, Orlando (USA), 2005: p. 591–600.
[24] R. Soderberg, L. Lindkvist, S. Dahlström, Computer-aided robustness analysis for compliant assemblies, Journal of Engineering Design. 17 (2006) 411–428.
[25] K. Xie, L. Wells, J.A. Camelio, B.D. Young, Variation propagation analysis on compliant assemblies considering contact interaction, Journal of Manufacturing Science and Engineering. 129 (2007) 934–942.
[26] G. Mandil, A. Deroschers, A. Rivière, Geometric requirement variations throughout the product lifecycle, in: ISBN 978-1-84821-276-3, Annecy (France), 2010: p. 521–542.
[27] S. Benichou, B. Anselmetti, Thermal dilatation in functional tolerancing, Mechanism and Machine Theory 46 (2011) 1575–1587.